Journal of Engineering Science and Technology
Vol. 11, No. 4 (2016) 458 - 475

HYGRO-THERMAL BEHAVIOUR OF POROUS BUILDING MATERIAL SUBJECTED TO DIFFERENT EXTERNAL TEMPERATURE AND HUMIDITY CONDITIONS

ALI CHIKHI[1,2,*], AZEDDINE BELHAMRI[2], PATRICK GLOUANNEC[3], ANTHONY MAGUERESSE[3]

[1]Département de Génie Civil, Faculté de Technologie,
Université Ferhat Abbes, Sétif 19000 Algeria
[2]Laboratoire de Génie Climatique, Faculté des Sciences de la Technologie, Université Constantine 1, 25000 Algeria
[3]Laboratoire d'Ingénierie des MATériaux de Bretagne, Université de Bretagne Sud, Rue de Saint Maudé, 56321 Lorient Cedex France
*Corresponding Author: a.chikhi@yahoo.fr

Abstract

This work is focused on the behaviour of a block of cement mortar, subjected to variable external temperature and humidity conditions. The porous building material sample is fitted inside a box, in which a heat exchanger is connected to a thermostatic bath. Three sequences of measurement are considered: (i) the response of the sample, when variations of temperature are applied; (ii) the air ranging between the exchanger and the non-isolated face of the mortar is continuously humidified, by injecting of sprayed water; (iii) the effect of simultaneously variation on temperature and humidity. A mathematical model representative of heat and mass transfer, in multiphasic medium (cement mortar), is developed in order to confront experimental and numerical results. Displacements of moisture and temperature fronts are observed and discussed. This study would enable us to understand the hygro-thermal behaviour of construction walls, to make an adequate design according to the climatic parameters and thus to improve the control of the energy used for heating.

Keywords: Cement mortar, Variable conditions, Experimentation, Modelling.

1. Introduction

Predicting the heat and moisture fields, within building envelopes, is of great importance to evaluate thermal comfort, energy consumption and durability of the construction.

Nomenclatures

c	Specific heat, $J.kg^{-1}.K^{-1}$
D_T	Mass transfer coefficient due to temperature gradient, $m^2.s^{-1}.K^{-1}$
D_S	Mass transfer coefficient due to saturation gradient, $m^2.s^{-1}$
D_{Tl}	Liquid phase transfer coefficient due to temperature gradient, $m^2.s^{-1}.K^{-1}$
D_{Tv}	Vapor phase transfer coefficient due to temperature gradient, $m^2.s^{-1}.K^{-1}$
D_{Sl}	Liquid phase transfer coefficient due to saturation gradient, $m^2.s^{-1}$
D_{Sv}	Vapor phase transfer coefficient due to saturation gradient, $m^2.s^{-1}$
D_{vap}	Diffusivity coefficient of the vapor in the air, $m^2.s^{-1}$
D_{eff}	Effective diffusivity coefficient of vapor, $m^2.s^{-1}$
Hr	Relative humidity, %
h_c	Convective heat transfer coefficient , $W.m^{-2}K^{-1}$
h_r	Radiative heat transfer coefficient,$W.m^{-2}.K^{-1}$
h_m	Mass transfer coefficient, $m.s^{-1}$
j	Mass flow, $kg.m^{-2}s^{-1}$
k	Intrinsic permeability, m^2
k_{rl}	Relative permeability
L_c	Characteristic length, m
L_v	Latent heat of vaporization, $J.kg^{-1}$
M	Molar mass, $kg.mol^{-1}$
P_c	Capillary pressure, Pa
P_v	Vapor pressure, Pa
P_{vsat}	Saturated vapor pressure, Pa
R	Gas constant, $J.mol^{-1}.K^{-1}$
S	Saturation coefficient
T	Temperature, K or °C
t	Time, s
w	Mass moisture content (kg of water/kg of porous material)

Dimensionless numbers

Bi	Biot number, $Bi = h_c L_c/\lambda$
Fo	Fourier number, $F_o=\alpha.t/(L_c)^2$
Pr	Prandtl number, $Pr=\gamma/a$
Sc	Schmith number, $Sc=\gamma/D_{vap}$
Gr	Grashof number (heat transfer), $Gr=g\Delta TL_c^3/(T_{film}\,\gamma^2)$
Gr_m	Grashof number (mass transfer), $Gr_m=g\Delta\rho L_c^3/(\rho\gamma^2)$

Greek Symbols

ε	Porosity
ρ	Density, $kg.m^{-3}$
λ	Thermal conductivity, $W.m^{-1}.K^{-1}$
α	Thermal diffusivity, $m^2.s^{-1}$
μ	Dynamic viscosity of water, $kg.m^{-1}s^{-1}$
γ	Kinematic viscosity, $m^2.s^{-1}$

Subscripts / Supercripts

a	Air

p	Partition (wall)
l	Liquid
v	Vapor
s	Solid

Most materials used in the construction of buildings are porous. A portion or possibly the totality of these pores is interconnected, making them permeable to the moisture. This moisture, in addition to the problems of durability which it is likely to cause [1-5], can also influence the thermal performances appreciably. Consequently, heat and mass transfer phenomena in building materials are strongly coupled.

Several studies have been conducted in order to make a more realistic analysis leading to reduced cost of energy consumption in buildings. In one of the projects a study of the relative humidity of the air in an office building was performed, taking into account the ability of the building materials to buffer the air humidity and to estimate the risk of condensation especially on the chilled ceiling. The results showed that optimizing the ventilation rate and buffering materials for target indoor moisture levels can lead to energy savings and to more stable indoor climates in terms of relative humidity [6]. This moisture depends on several factors, among them the sorption or desorption of the solid materials.

For over a decade, fairly comprehensive tools for transient building energy simulation have been well established; but these tools are relatively weak to describe the process of transferring moisture in buildings. Most of these tools do not take into account the moisture flow between air and porous surfaces.

In spite of the broad use of cement mortar in construction field, its hygro-thermal behaviour is not clarified satisfactorily, especially under the particular conditions of its use.

The present study involves raising measurements on an instrumented block of cement mortar subjected to changes of temperature and moisture. A coupled heat and mass transfer model is applied to predict the heat and moisture distributions during the processes. Measurements are compared with the numerical results in order to validate them. A study of the heat flux sensitivity on the surface of the sample with respect to the thermal transfer mode is also carried out.

This work is a continuity of a previous study conducted by Chikhi et al. [7]. The same methodology is followed, but in this event, other devices are added to the experimental system in order to control, at the same time, the temperature and relative humidity of the ambient air of the experiment.

2. Experimental study

2.1. Studied material

Cement mortar is a building compound created by mixing sand and a selection of aggregates with a specified amount of water. Itcan be used for a number of applications.

Mortar has been used for centuries as a means of adhering bricks or concrete blocks to one another. It continues to be used in many different types of

construction. Professional building projects often employ mortar as the binder between bricks in walls, fences, and walkways. Around the house, it is often employed to make quick repairs in patio slabs and reset loosened stones or bricks in a walkway or retaining wall.

Cement mortar also makes an excellent medium for creating a smooth surface to walls made from bricks and other forms of masonry. It is applied with the use of a trowel and then smoothed into position. Often, the application is conducted in more than one coat, making it possible to slowly achieve a covering that adheres properly to the wall surface. The mortar may be tinted in order to add a small amount of color to the façade or paint can be added as a topcoat at a later date.

The ingredients in cement mortar vary somewhat, depending on the manufacturer specifications. For this study, the detained composition is described in Table 1.

Table 1. Initial composition of studied material.

	Cement	Sand	Water	Water/Cement
Mass fraction	0.222	0.666	0.111	0.5

After mixing the various components (sand, cement and water), the mortar is versed in a wooden plane-parallel mould of 25cm on sides and 5cm depth.

With the same mixture, other samples of smaller size (13x13x2 cm^3) were made. These plates were used for the measurement of some thermo physical properties of the material. These properties include thermal conductivity, specific heat and density Table 2. The porosity is drawn from Da Chen [8].

Table 2. Properties of studied material for a temperature ranging between 0 and 50°C.

Density ($kg.m^{-3}$)	Porosity (-)	Thermal conductivity ($W.m^{-1}.K^{-1}$)	Specific heat ($J.kg^{-1}.K^{-1}$)
2200	0.18	1.6	850

2.2. Description of measurement device

A sample of cement mortar, kept in its wooden mould, was insulated from all sides except on a vertical face in order to approaching the adiabatic conditions and thus obtaining a one-dimensional heat flow. This block is fitted in an upright position, inside a box, in which a heat exchanger is fixed and connected by piping to a thermo-stated bath so as to control the temperature of the water-glycol mixture, circulating inside the circuit. Humidification is obtained by spraying water injection in the air ranging between the exchanger and the non-isolated face of the sample. Moisture and temperature sensors, distributed on the various elements of the experimental bench, are connected to a station of acquisition as shown in Fig. 1.

The measurement of the temperatures of isolated sides of the sample "*T2* to *T6*" is ensured by thermocouples stuck to the wooden mould, that of the face in direct contact with the air "*T7*" by another, stuck to the mortar, temperature "*T1*" by a jacketed thermocouple in stainless, inserted into the material during the

casting as shown in Fig. 1 and Table 3. In parallel, to know the degree of temperature and humidity inside the sample, three sensors "*S1* to *S3*" were inserted in the sample at 1 cm of the bottom, at the medium and at 1 cm of surface, respectively. To apprehend the exchanges at the level of the two faces subjected to the convection (exchanger and block), some measurements of humidity and temperature of the air are realized by a sensor placed in space separating the two faces (*S4*). Lastly, thermocouples are stuck to the surface of the exchanger; the average of their measurements gives the temperature "*T8*".

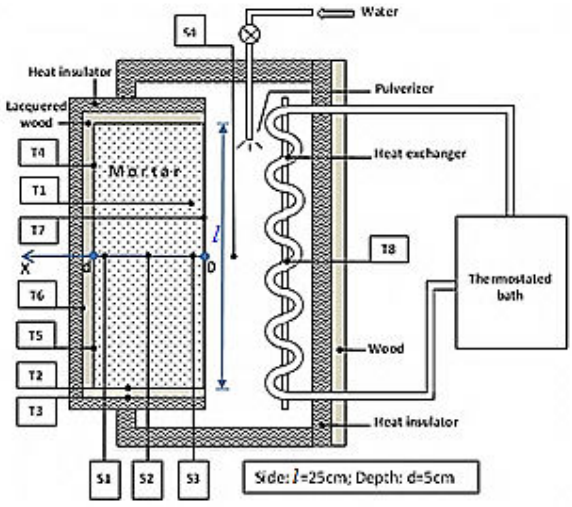

Fig. 1. Block diagram of the measurement device and sensors implantation.

The principle diagram of the measurement device and the sensors implantation are shown in Fig. 1. Table 3 gives the designation of the sensors and their position.

All thermocouples T_i, i=1, 2,…,7, used in this experiment, are type (K) and measure temperature in °C, Their measurement accuracy is 0.2°C; their measurement range is -100°C to 1370°C.

All sensors S_i, i=1, 2,…, 4 are "Sensirions" kind and measure T [° C] + Hr [%]. They combine humidity and temperature sensor on a single chip with reduced dimensions. They have excellent accuracy while remaining economical. Capacitive sensors fully calibrated, provide a digital output signal and do not need to be calibrated, they are characterized by their long-term stability. The Sensirion sensor with four-pin standard dimensions make both solderable and pluggable.

Technical Specifications
Measuring range: 0 to 100% *Hr*
Temperature range: -40 to +125 ° C
Measurement accuracy: (0.4 ° C) ± 3%
Length: 19.5 mm
Width: 5.1 mm
Height: 3.1 mm

Table 3. Designation and position of the connected sensors.

Designation	Position	Designation	Position
T1	Into the mortar at x= 1 cm	**T7**	Surface of the sample (x=0)
T2	Interface mortar-wood	**T8**	Surface of the heat exchanger
T3	Interface wood-insulator	**S1**	Into the mortar at x= 4cm
T4	Interface mortar-wood (x=5 cm)	**S2**	Into the mortar at x= 2.5cm
T5	Interface mortar-wood (x=5 cm)	**S3**	Into the mortar at x= 1 cm
T6	Interface wood-insulator	**S4**	In the air

3. Modeling

3.1. Presentation of the physical model

Several models were established to describe the coupled heat and mass transfer phenomena in porous media. The first tests of modeling have only taken into account the transfer in the vapor phase in order to study the risks of condensation in the walls; they suppose negligible the transfer in liquid phase. However, the incomplete character of these approaches led the researchers to elaborate some works describing in a more precise way this phenomenon of coupled transfers [9-12].

The model developed by "Philip and De-Vries" in 1957 and used by Crausse et al. [13], is chosen to conceive the present work. It allows a good description and faithfully restores most of the phenomena observed in laboratory for homogeneous mediums, isotropic, slightly hygroscopic [10].

In the case of a one-dimensional representation of the exchanges, and in the case of following assumptions of modeling:

- the solid phase constituting the porous media is homogeneous, non-deformable and isotropic,
- the various phases are in thermal and hygroscopic balance,
- the gas phase obeys the law of perfect gases,
- there is no chemical reaction,
- the density of the liquid phase is constant,
- the effects of gravity are neglected,

So, the system of equations of the model is written:

$$\begin{cases} \varepsilon \, {\partial S}/{\partial t} = \nabla.[\varepsilon(D_{Sl} + D_{Sv})\nabla S + (D_{Tl} + D_{Tv})\nabla T] & (1) \\ \rho c \, {\partial T}/{\partial t} = \nabla.(\lambda \nabla T) + \nabla.(\rho_l L_v D_{Tv} \nabla T + \varepsilon \rho_l L_v D_{Sv} \nabla S) & (2) \end{cases}$$

The saturation coefficient (S) is defined like the ratio of the volume of water contained in the pores on the volume of the open pores. It is related to the mass moisture content by the following relation [14]:

$$S = {w\rho_s}/{\varepsilon\rho_l} \quad (3)$$

The discretization of differential equations is carried out by implicit finite volume method, it is well suited for transient problems involving large values of time and it is characterized by its stability and convergence [15].

After discretization, one obtains two equations of the form:

$$ai\ Fi\ =\ bi\ Fi+1\ +\ ci\ Fi-1\ +\ di \tag{4}$$

F can be saturation coefficient S or temperature *T*.

Coefficients:a_i, b_i, c_i and d_i depends on several parameters among which appear D_{sl}, D_{sv}, D_{Tl} *and* D_{Tv} which themselves depend on the temperature *T* and the saturation coefficient S at the same time.

The function *Fi* depends on two neighboring functions F_{i+1} and F_{i-1}. When pooling these equations, a tri diagonal matrix is obtained.

For the resolution, we used an algorithm called TDMA (Tri Diagonal Matrix Algorithm) to make the matrix into a bi diagonal matrix. The system of equations is solved by back substitution (Gauss elimination method). Nonlinearity is treated for each system by a convergence test on each variable. In each loop, the characteristics depending on the corresponding variable are recomputed for each iteration. The overall convergence test performed on the two variables of the system can handle the coupling system of equations. The cycle is repeated until the difference between two successive values of the temperature and the saturation respects the overall convergence criterion. The mesh used is a regular grid and the model is programmed in FORTRAN.

3.2. Mass transfer coefficient due to saturation gradient D_S

D_S is the sum of the liquid water transfer coefficient and that of the vapor water under the effect of a saturation gradient:

$$D_S = D_{Sl} + D_{Sv} \tag{5}$$

D_{Sl} and D_{Sv} are calculated from the following expressions [16] and [17]:

- ✓ *Liquid water transfer coefficient:*

$$D_{Sl} = \frac{k.krl}{\varepsilon.\mu_l}\left(-\partial P_c/_{\partial S}\right) \tag{6}$$

Several authors proposed empirical relations to determine the permeability relating to water and gases. For cementing materials, Laghcha [18] shows that the permeability related to the liquid can be determined in the following way:

$$k_{rl} = \sqrt{S}\left[1-\left(1-S^{1/m}\right)^m\right]^2 \ ; m = 1/2.1 \tag{7}$$

In the same way, the capillary pressure (P_c) can be calculated according to saturation coefficient [19]:

$$P_c = a(S^{-2.27}-1)^{(1-m)}\ ;\ a = 20.45.10^6 \tag{8}$$

- ✓ *Vapor water transfer coefficient:*

$$D_{Sv} = \frac{D_{eff}MP_{vsat}}{\rho_l RT\varepsilon}\left(\partial f/_{\partial S}\right) \tag{9}$$

where D_{eff} is the effective coefficient of diffusion and f is a function which depends on capillary pressure and temperature, they are calculated as follows [16]:

$$D_{eff} = D_{vap}(1 - S^2)[\varepsilon(1 - S)]^{4/3} \quad (10)$$

$$f = exp\left(-{P_c M}/{\rho_l RT}\right) \quad (11)$$

Lastly, the saturating vapor pressure P_{vsat} is determined by the following relation:

$$P_{vsat} = 611exp\left(\frac{17.27\,T}{T+237.3}\right); \text{ } P_{vsat} \text{ in [Pa] and T in [°C]} \quad (12)$$

3.3. Mass transfer coefficient due to temperature gradient D_T

D_T is the sum of the liquid water transfer coefficient and that of the vapor water under the effect of a temperature gradient:

$$D_T = D_{Tl} + D_{Tv} \quad (13)$$

D_{Tl} and D_{Tv} are calculated from the following expressions [14]:

- ✓ *Liquid water transfer coefficient:*

$$D_{Tl} = \rho_l \frac{k.krl}{\mu_l}\left(-{\partial P_c}/{\partial T}\right) \quad (14)$$

The capillary depression (- P_c) is connected to the temperature and relative humidity via the well-known equation of Kelvin:

$$-P_c = {RT\rho_l . ln(H_r)}/{M} \quad (15)$$

- ✓ *Vapor water transfer coefficient:*

$$D_{Tv} = D_{eff}\left(\frac{M_a M_v}{MRT}\right){\partial P_v}/{\partial T} \quad (16)$$

The vapor pressure is calculated from the following expression:

$$P_v = H_r P_{vsat} \quad (17)$$

3.4. Boundary conditions

- ➢ ***Mass Transfer***

At x= 0:

$$-\left(\varepsilon D_S\, {\partial S}/{\partial x} + D_T\, {\partial T}/{\partial x}\right)_{x=0} = \frac{h_m}{\rho_l}\left(\rho_{v,\infty} - \rho_{v,x=0}\right) \quad (18)$$

At the other limits (at $x = d$), surface is supposed to be impermeable (water proof lacquered wood), the mass flow, which crosses it, is thus null.

➢ ***Heat Transfer***

At x = 0:

$$-\left(\lambda\, {}^{\partial T}/_{\partial x}\right)_{x=0} - (L_v j_v)_{x=0} = (h_c + h_r)(T_\infty - T_{x=0}) + L_v h_m\left(\rho_{v,\infty} - \rho_{v,x=0}\right) \quad (19)$$

On the bottom, on the insulated face, i.e., when x=d, the temperature is imposed. It is the average temperature measured by the thermocouples "*T4*" and "*T5*".

➢ In order to carry a comparison (numeric simulation /experiment), both temperature and relative humidity of the air are extracted each step of time from the experiment's real conditions.

3.5. Transfer coefficients

➢ ***Convective heat transfer coefficient***

The Convective heat transfer coefficient is calculated from Nusselt number:

$$h_c = \frac{\overline{N_u}\lambda}{L} \quad (20)$$

For natural convection, the dimensionless number "Nusselt" is a function of Grashof and Prandtl:

In the case of a laminar flow: $10^4 \leq Gr.Pr \leq 10^9$

$$\overline{Nu} = 0.59(Gr.Pr)^{0.25} \quad (21)$$

For a turbulent flow: $10^9 \leq Gr.Pr \leq 10^{13}$

$$\overline{Nu} = 0.021(Gr.\mathrm{Pr})^{2/5} \quad (22)$$

➢ ***Radiative heat transfer coefficient***

The density of heat flux transferred by radiation is given by the following relationship:

$$q_r = \varepsilon\sigma(T_s^4 - T_e^4) \quad (23)$$

σ: Stephan Boltzmann constant (σ=5.67x10^{-8} W.m^{-2}.K^{-4})
ε: emission coefficient of the surface.
Ts: surface temperature of the sample.
Te: surface temperature of the heat exchanger.
After linearization, we obtain:

$$q_r = h_r(T_s - T_e) \quad (24)$$

with: $h_r = 4\varepsilon\sigma T_m^3$ (25)

T_m is the mean temperature of the two surfaces.

➢ ***Mass transfer coefficient***

The mass transfer coefficient is calculated from Sherwood number:

$$h_m = \frac{\overline{Sh} D_{vap}}{L} \quad (26)$$

For natural convection, the dimensionless number "Sherwood" is a function of Grashof and Schmith:

In the case of a laminar flow: $10^4 \leq Gr_m.Sc \leq 10^9$

$$\overline{Sh} = 0.59(Gr_m.Sc)^{0.25} \quad (27)$$

For a turbulent flow: $10^9 \leq Gr_m.Sc \leq 10^{13}$

$$\overline{Sh} = 0.021(Gr_m.Sc)^{2/5} \quad (28)$$

3.6. Initial conditions

For the same reason, the initial conditions applied to the model are also extracted from the real conditions of the experiment.

4. Results and Discussion

4.1. Measurement sequences

Figures 2, 3 and 4 present the evolution of relative humidity and temperature for the three sequences of measurement. In the first one, variations of temperature of the heat exchanger are applied. In the second sequence, the air ranging between the exchanger and the non-isolated face of the mortar is continuously humidified, by injecting of sprayed water. In the last sequence, variations on temperature and humidity of the air are applied simultaneously (by heat exchanger and pulverizer at the same time).

In Fig. 2(b), the temperature remains constant until time 20h. By applying a fall of temperature in the heat exchanger, one observes a fall of the air's temperature, followed by a fall of temperature in the various points of measurement. This fall generates an elevation of the air's relative humidity and then that of the interior of the material as shown in Fig. 2(a) (with x=1 cm). In this first sequence, the response of *Hr* within the block is very slow because *Hr* of the air was initially slower than *Hr* of material and also was in phase of descent as shown in Fig. 2(a) (from 10 to 20 hours). Moreover, the fall of the temperature did not involve a significant elevation of *Hr* of the air. In both other cases where humidification is ensured by pulverization, the response of *Hr* within material is more quick as shown in Fig. 3 (pulverization and maintaining of heat exchanger at a standstill) and Fig. 4 (pulverization plus variation in temperature of exchanger).

It should be highlighted that the fluctuations observed of the air's relative humidity are mainly due to the difficulty of controlling this one (Hr of the air), especially after the starting of the thermo-stated bath as shown in Fig. 4.

It should be noted also that the weak variation in temperature between the surface of the sample and the bottom (Figs. 2(b), 3(b) and 4(b)) is due to the great value of thermal conductivity (1.6 W m^{-1} K^{-1}) and to a thickness of the relatively small block (5 cm). Moreover, the transfer is carried out at a temperature close to that of the wet bulb corresponding to the conditions of test, for example 30.9°C

for a dry temperature of 35°C and a relative humidity of approximately 75% as shown in Figs. 4(a) and (b) (at t = 65 hours).

The conditions of the experiment, the dimensions and the thermal conductivity of the sample make it possible to estimate the number of *Biot*. Its value is lower than 0.18, which explains an internal profile, almost constant.

The advance of the observed thermal front indicates approximately a time lag of 5h as shown in Fig. 2(b). The number of Fourier, deduced from the experimental conditions, is around 7. The thermal diffusivity, calculated for this material and under the experimental conditions used, is equal to 8.56 10^{-7} m^2/s.

The profile of the relative humidity, measured inside the sample, indicates also a delay of the same order as that observed for the temperature. On the other hand, near the surface, the response is most notable and increasing the humidity is higher, which is probably due to the combination of the effect of humidity, temperature of the air, and transport of internal moisture.

The front of displacement of moisture in material is more visible during the increase of the air humidity as shown in Figs. 3(a) and 3(b). The material temperature follows the evolution of the temperature of the outside air with a delay, already observed in the previous sequence, but the fluctuations are not as important as the other results.

In the last series (Figs. 4(a) and (b), the combined effect of two parameters: temperature and humidity of the air, can observe the progress of the internal front of temperature and humidity. Measures of internal humidity (as shown in Fig. 4(a)) indicate that the material reacts to the fluctuations of the air humidity with a more significant delay for the deepest points than for those close to surface.

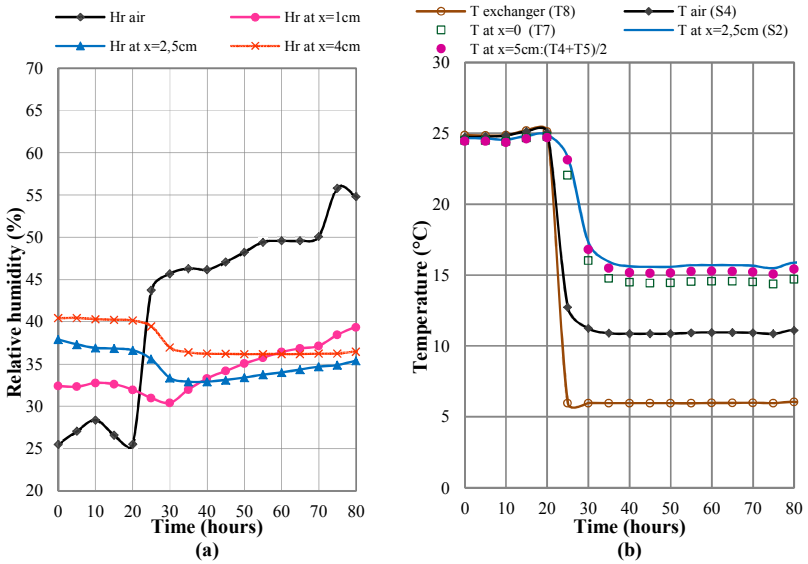

Fig. 2. Variation of relative humidity and temperature during the first sequence of measurement.

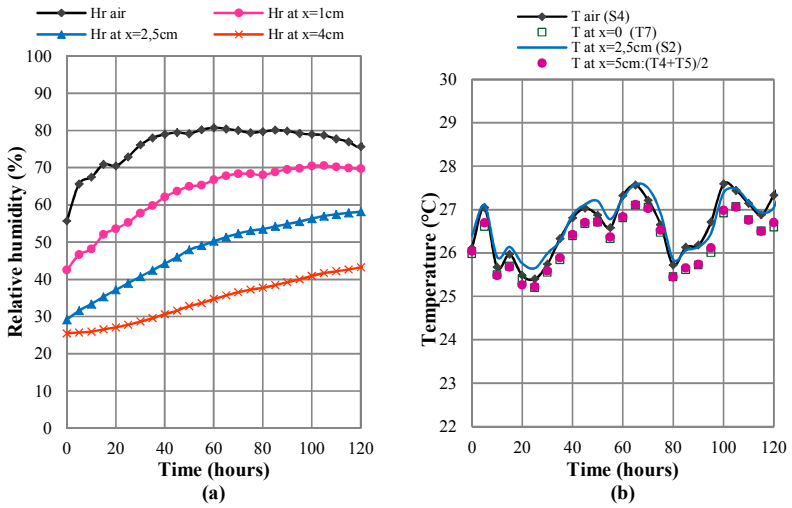

Fig. 3.Variation of relative humidity and temperature during the second sequence of measurement.

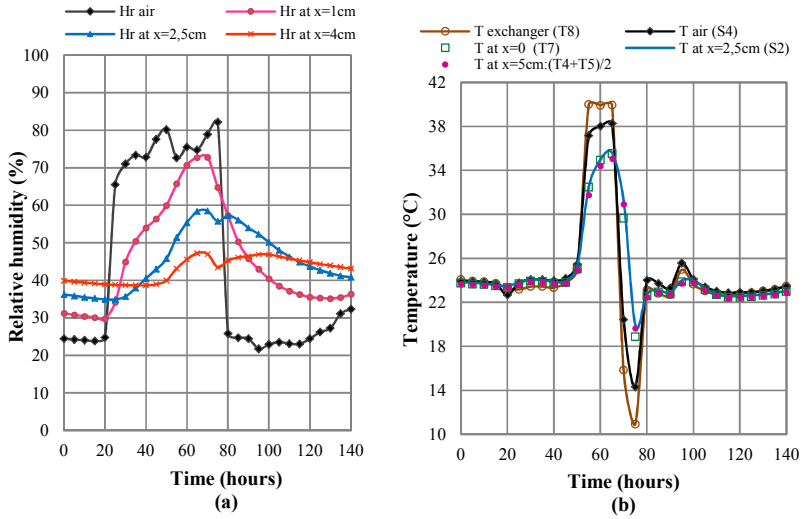

Fig. 4. Variation of relative humidity and temperature during the third sequence of measurement.

4.2. Evolution of relative humidity and temperature

In order to reproduce the experimental results and to validate the model suggested to simulate the behavior of this material, aseries of simulation reproducing the experimental conditions was carried out.

Figures 5, 6 and 7 show the evolution according to the time of the relative humidity and the temperature of the air as well as various depths of the block. A

comparison was carried out between the measured values and those calculated by the model.

For the relative humidity (activity), there is a good concordance when it is a matter of varying only one parameter of the air - temperature or relative humidity Figs. 5(a) and 6(a) and less concordance in the third case as shown in Fig. 7(a), the simultaneous and very quick fluctuations of both temperature and *Hr* of the air are the principal cause of the small differences observed. But, such a case does not represent the real climatic conditions.

For the change of temperature, there is also a very good concordance between the computed values and those measured as shown in Figs. 5(b), 6(b) and 7(b). The coincidence of certain curves is due to the difficulty in imposing in experiments a significant variation in temperature between the surface and the bottom of sample.

Figure 5.a reproduces the first sequence of measurements. It shows a slight shift in the early stage (before 20h) and for the statements in-depth of the sample, which is probably due to the fluctuations of the air humidity. Nevertheless, the model reproduces development and displacement of moisture and temperature fronts as shown in Fig. 5(b); we can thus distinguish the delayed response about 5 hours compared to the variation of the applied conditions.

Figures 6 and 7 confirm the preceding remarks, in particular the sensitivity of the model to variations of humidity of the surrounding air. The shifts are observed for the deepest points of the sample. Improvements on obtaining internal transport properties could be envisaged to refine the model results.

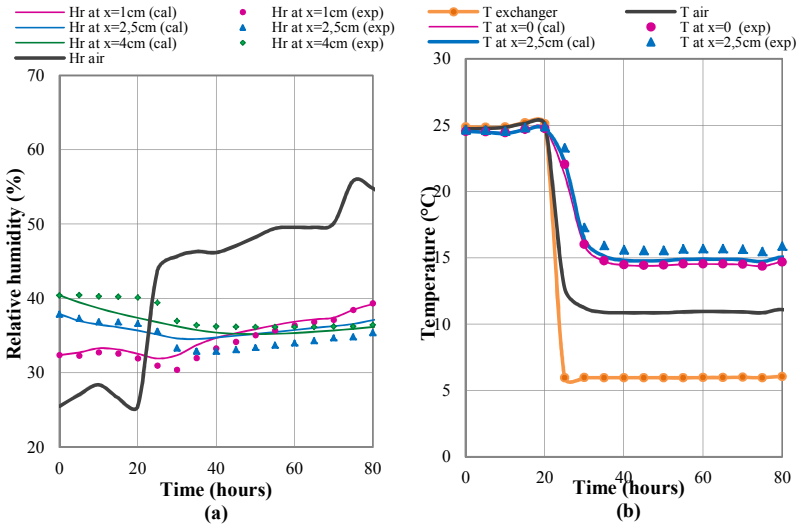

Fig. 5. Evolution of relative humidity and temperature: comparison between model and experiment (Sequence 1).

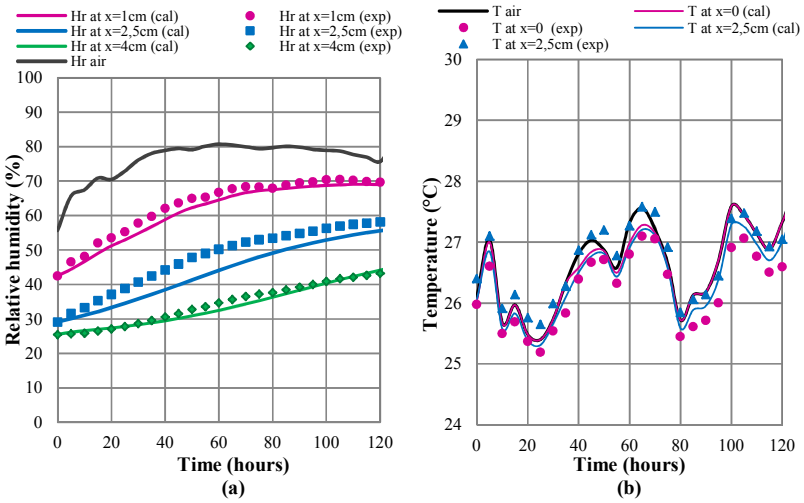

Fig. 6. Evolution of relative humidity and temperature: comparison between model and experiment (Sequence 2).

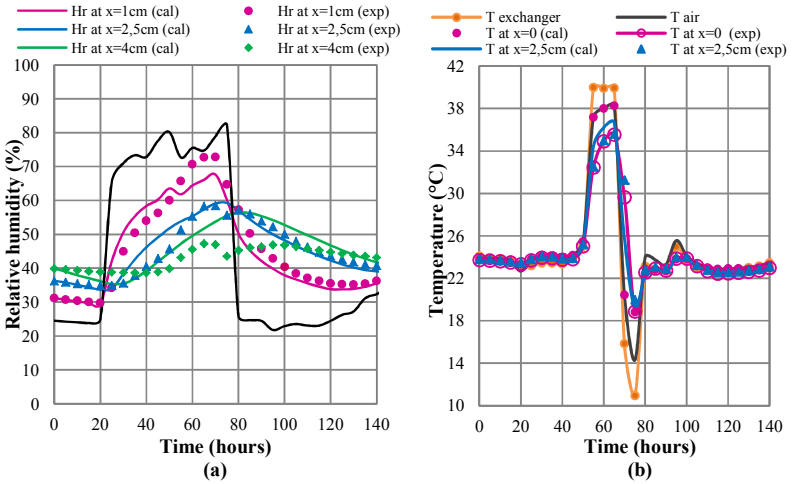

Fig. 7. Evolution of relative humidity and temperature: comparison between model and experiment (Sequence 3).

4.3. Profile of relative humidity and temperature

In order to evaluate the quality of the results obtained by the model, a space-time confrontation between the profiles of temperature and moisture is presented for the three studied cases and for three times chosen arbitrarily as shown in Figs. 8, 9 and 10. The comparisons show a maximum shift estimated at 6% for the relative humidity Fig. 9(a) and 1.5°C for the temperature Fig. 8(b), which allows concluding on good capabilities of the model to predict the material behaviour under variable hygro-thermal conditions.

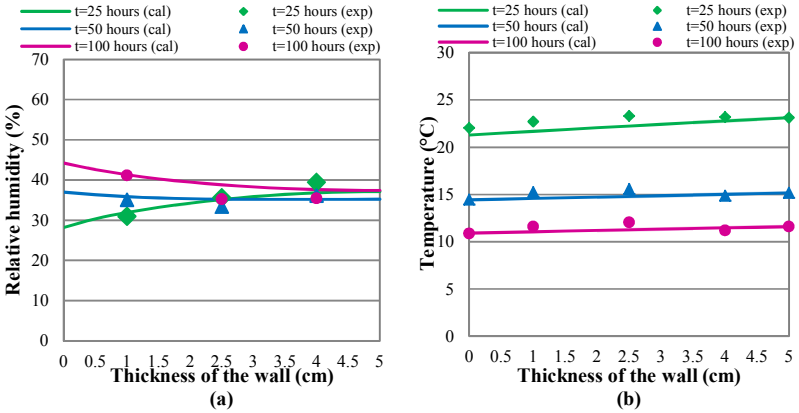

Fig. 8. Profile of relative humidity and temperature: comparison between model and experiment (Sequence 1).

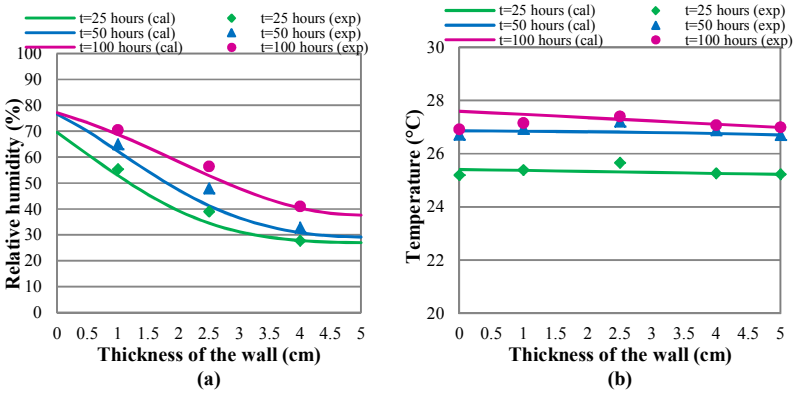

Fig. 9. Profile of relative humidity and temperature: comparison between model and experiment (Sequence 2).

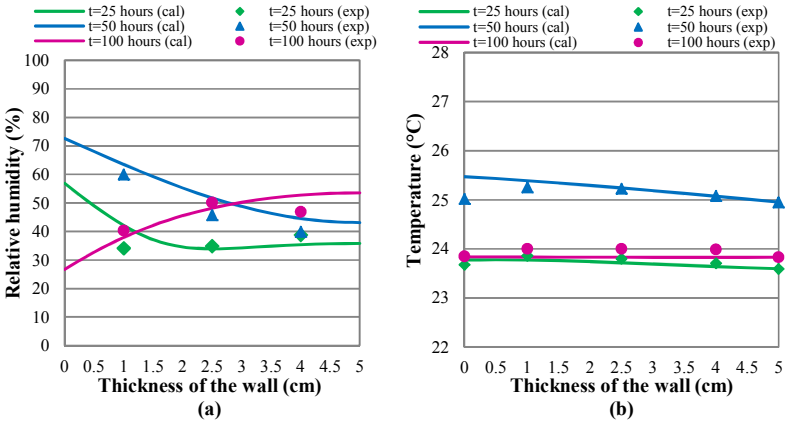

Fig. 10. Profile of relative humidity and temperature: comparison between model and experiment (Sequence 3).

4.4. Heat flux on the surface

To investigate the sensitivity of heat flux on the surface with respect to the thermal transfer mode, three cases were treated. The first case was by considering convection and radiation between the surface of the mortar and that of the exchanger. The second was by neglecting the convection and the last was by neglecting the radiation. The test conditions are similar to those of the third measuring sequence (simultaneous variation of the temperature and relative humidity). Figure 11 shows that, in this study, the convection can be neglected and the radiation flux coincides with that of the first case. That is due to the insulation of the space between the two faces and the small thickness of the airspace (approximately 4 cm).

The result of this test allows neglecting, without making a mistake, convection between two layers of a building wall separated by an air space in the case of the hygrothermal behaviour study of multilayered walls.

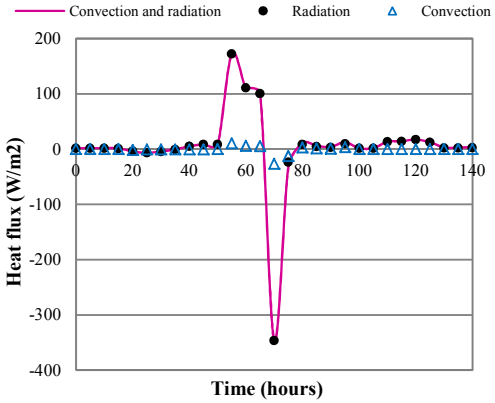

Fig. 11. Heat flux on the surface (Sequence 3); correspondence with the Fig. 4(b) and Fig. 7(b).

5. Conclusions

The study of coupled transfer of heat and moisture in porous media such as building materials is very important to improve their composition and performance.

- This work presents numerical investigation to predict experimental measurements, mainly temperature and relative humidity under real variables conditions.
- The experiments carried out made it possible to observe the response of the material to varying temperature and moisture conditions. The material reacts to changes in the parameters of the outside air. The influence of air humidity is much more important for near-surface points.
- The simulation model adopted in this study allows us to approach, with satisfactory accuracy, the real profiles of internal moisture and temperature during the process.

- The mass transfer coefficient used is not obtained from direct measurements, but it is built, taking into account specific properties of the material, which are measured independently. It depends on saturation and temperature.
- This model can be applied to other types of building materials under real conditions of use. It is therefore possible to improve the thermal performance and thus to save the energy used, especially in heating and air conditioning, while acting either on the composition of the wall or on its thickness.

References

1. Mendes, N.; Winkelmann, F.C.; Lamberts, R.; and Philippi, P.C. (2003). Moisture effects on conduction loads. *Energy and Buildings*, 35(7), 631–644.
2. Jerman, M.; and Cerny, R. (2012). Effect of moisture content on heat and moisture transport and storage properties of thermal insulation materials. *Energy and Buildings*, 53, 39-46.
3. Khan, M.I. (2002). Factors affecting the thermal properties of concrete and applicability of its prediction models. *Building and Environment*, 37, 607-614.
4. Wyrwal, J.; and Marynowicz, A. (2002). Vapour condensation and moisture accumulation in porous building wall. *Building and Environment*. 37(3), 313-318.
5. Dal Pont, S. (2004). *Lien entre la perméabilité et l'endommagement dans les bétons à haute température*. Ph.D. Thesis. Ecole Nationale des Ponts et Chaussées, France.
6. Rode, C.; and Woloszyn, M. (2007). Whole Building Heat, Air and Moisture Response in IEA. *Annex 41, ASHRAE.*
7. Chikhi, A.; Belhamri, A.; Glouannec, P.; Magueresse, A. (2014). Experimental Study and Modeling of Coupled Heat and Moisture Transfers in Cement Mortar. *International Journal of Engineering and Applied Sciences (IJEAS),* 6 (1), 14-27.
8. Da Chen. (2005). *Modélisation du comportement hydromécanique d'un mortier sous compression et dessiccation*, Ph.D. Thesis. University of Lille, France.
9. Whitaker, S. (1977). Simultaneous heat, mass and momentum transfer in porous media – A theory of drying in porous media. *Advances in Heat Transfer*, 13, 119-200.
10. Bories, S. (1982). Transferts de chaleur et de masse dans les matériaux, analyse critique des différents modèles mathématiques utilisés. *L'humidité dans le bâtiment, Séminaire de l'UNESCO*. France, 23-25 Novembre, 13-32.
11. Hagentoft, C.E.; Kalagasidis, A.S.; Adl-Zarrabi, B.; Roels, S.; Carmeliet, J.; Hens, H.; Gruenwald, J.; Funk, M.; Becker, R.; Shamir, D.; Adan, O.; Brocken, H.; Kumaran, K.; and Djebbar, R. (2004). Assessment method of numerical prediction models for combined heat, air and moisture transfer in building components: benchmarks for one-dimensional cases. *Journal of Thermal Envelope and Building Science*, 27 (4), 327–352.
12. Mendes, N.; Philippi, P.C.; and Lamberts, R. (2002). A new mathematical method to solve highly coupled equations of heat and mass transfer in porous media. *International Journal of Heat and Mass Transfer*, 45, 509-518.

13. Crausse, P.; Laurent, JP. ; and Perrin, B. (1996). Influence des phénomènes d'hystérésis sur les propriétés hydriques de matériaux poreux. *Revue Générale de Thermique*, 35, 95-106.
14. Salagnac, P.; Glouannec, P.; and Lecharpentier, D. (2004). Numerical modeling of heat and mass transfer in porous medium during combined hot air, infrared and microwaves drying. *International Journal of Heat and Mass Transfer*, 47, 4479–4489.
15. Patankar, S.V. (1980). Numerical Heat Transfer and Fluid Flow, Chapter four: Heat Conduction. *Hemisphere Publishing Corporation*, 41-77.
16. Belhamri, A. (2003). Characterization of the first falling rate period during drying of a porous material. *Drying Technology*, 21(7), 1235-1252.
17. Belhamri, A. (1992). *Etude des transferts de chaleur et de masse à l'interface d'un milieu poreux au cours du séchage*. Ph.D. Thesis. University of Poitiers, France.
18. Laghcha, A. (2006). *Contribution à l'étude des transferts gazeux et liquide au sein des parois en béton endommagées sous sollicitation thermo-hydrique*. Ph.D. Thesis. Ecole doctorale des Sciences de l'Ingénieur, Lyon, France.
19. Billard, Y. (2003). *Contribution à l'étude des transferts de fluides au sein d'une paroi en béton.* Ph.D. Thesis. Ecole doctorale des Sciences de l'Ingénieur, Lyon, France.